Microporous and Mesoporous Materials 360 (2023) 112699

Contents lists available at ScienceDirect

Microporous and Mesoporous Materials

journal homepage: www.elsevier.com/locate/micromeso

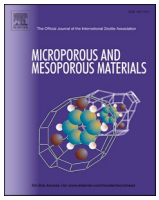

Guest-induced structural deformation in Cu-based metal-organic framework upon hydrocarbon adsorption

Azahara Luna-Triguero [a,b,*,1], Eduardo Andres-Garcia [c,d,1], Pedro Leo [c,e,**], Willy Rook [c], Freek Kapteijn [c]

[a] Energy Technology, Department of Mechanical Engineering, Eindhoven University of Technology, P.O. Box 513, 5600 MB, Eindhoven, the Netherlands
[b] Eindhoven Institute for Renewable Energy Systems (EIRES), Eindhoven University of Technology, PO Box 513, Eindhoven, 5600 MB, the Netherlands
[c] Catalysis Engineering, ChemE, TUDelft, Van der Maasweg 9, 2629 HZ, Delft, the Netherlands
[d] Instituto de Ciencia Molecular (ICMol), Universidad de Valencia, c/Catedrático José Beltrán, 2, Paterna, 46980, Spain
[e] Department of Chemical and Environmental Technology, Rey Juan Carlos University, Calle Tulipán s/n, 28933, Móstoles, Spain

ARTICLE INFO

Keywords:
Adsorption
Flexibility
Hydrocarbons
Open metal sites
Separation

ABSTRACT

In a world where capture and separation processes represent above 10% of global energy consumption, novel porous materials, such as Metal-Organic Frameworks (MOFs) used in adsorption-based processes are a promising alternative to dethrone the high-energy-demanding distillation. Shape and size tailor-made pores in combination with Lewis acidic sites can enhance the adsorbate-adsorbent interactions. Understanding the underlying mechanisms of adsorption is essential to designing and optimizing capture and separation processes. Herein, we analyze the adsorption behaviour of light hydrocarbons (methane, ethane, ethylene, propane, and propylene) in two synthesized copper-based MOFs, Cu-MOF-74 and URJC-1. The experimental and computational adsorption curves reveal a limited effect of the exposed metal centers on the olefins. The lower interaction Cu-olefin is also reflected in the calculated enthalpy of adsorption and binding geometries. Moreover, the diamond-shaped pores' deformation upon external stimuli is first reported in URJC-1. This phenomenon is highlighted as the key to understanding the adsorbent's responsive mechanisms and potential in future industrial applications.

1. Introduction

Natural Gas (NG) demand accounts for the highest fuel growth rate, and its consumption is expected to surpass coal's in 2030 [1]. Although NG is generally considered clean energy, it is not free of impurities – such as water, CO_2 and other hydrocarbons – that need to be removed by energy intensive separation processes [2]; consequently, a large amount of the world's current natural gas reserves are not available for being economically unprofitable [3]. In addition, the contribution of methane to the greenhouse effect should not be underestimated due to its elevated global warming potential (GWP) [4].

Propane/propylene separation is considered the most challenging separation in the chemical engineering industry for two main reasons: i) the similarities of the components in the mixture; ii) the high value of the feedstock involved in the process [5–7]. Both ethylene and propylene are two of the most important feedstocks in the chemical industry, with multiple applications in the refinery, and used as building block in the production of some of the most common chemicals and polymers. Although these alkenes are usually obtained in globally equimolar mixtures with their corresponding alkane (ethane and propane), industrial purity requirements demand new energy efficient separation techniques. Adsorption-based separation using porous materials is the technology to reach the required high purity (99.95 mol% ethylene [8]; 99.5 mol% propylene) [9], avoiding the high capital/-operational costs of the energy-demanding cryogenic distillation [10].

Metal-Organic frameworks (MOFs), a sub-class of porous coordination polymers (PCPs), are hybrid organic-inorganic porous materials well known for their promising structural properties such as high surface area, pore volume, and relatively high thermal and chemical stability. Accordingly, MOFs are being currently explored in a wide range of

* Corresponding author. Energy Technology, Department of Mechanical Engineering, Eindhoven University of Technology, P.O. Box 513, 5600 MB, Eindhoven, the Netherlands.
** Corresponding author. Department of Chemical and Environmental Technology, Rey Juan Carlos University, Calle Tulipán s/n, 28933, Móstoles, Spain.
E-mail address: a.luna.triguero@tue.nl (A. Luna-Triguero).
[1] ALT (computational) and EAG (experimental measurements) share first authorship with equal contribution.

https://doi.org/10.1016/j.micromeso.2023.112699
Received 30 March 2023; Received in revised form 1 June 2023; Accepted 8 June 2023
Available online 11 June 2023

applications such as gas sequestration and separation [11,12], energy storage [13], drug or biomolecule release [14,15], and heterogeneous catalysis [16].

Among the above mentioned properties, it is worth highlighting the chemical and functional tunability; the abundant number of organic ligands, metals and metallic clusters, crystallization conditions, and post-synthesis modifications allow almost infinite combinations [17–21].

Currently, the Cambridge structural database is the platform with more indexed MOFs, and the number of synthesized materials is growing exponentially [22,23]. The vast majority of reported MOFs can be classified as the second generation; robust frameworks with permanent porosity considered as rigid porous materials. On the other hand, structural flexibility is a desirable property that can be exploited for different applications and can theoretically be used for gas separation [24–28], although this has been rarely explored for mixtures since their performance is hard to measure and predict [29,30]. MOFs presenting framework flexibility, reversible structural changes upon external stimuli, are known as soft porous crystals (SPCs), the third generation of MOFs [31]. Only about 100 structures are reported to exhibit reversible phase transitions; however, it is a highly influential factor in understanding the underlying adsorption and diffusion mechanisms and performance prediction [32,33]. The influence of flexibility on the adsorption behaviour in MOFs has been reported in several studies. Flexible MOFs can undergo structural changes upon adsorption, enhancing capacity and selectivity for hydrocarbons. Maes et al. reported that MIL-53(Al) exhibited a higher separation capacity for styrene/methylbenzene mixture than its rigid counterpart, MIL-47(V) [34]. Similarly, UTSA series are found to increase acetylene/ethene separation when exchanging rigid by flexible organic linkers [35]. A positive effect was also reported on the separation of acetylene in fumarate [36]. The temperature-dependent swelling of Mn-*dhbq* is used to effectively separate hexane isomers from a ternary mixture [37]. On the other hand, ZIF-8 and ZIF-7 exhibited reverse ethane/ethene selectivity attributed to the framework flexibility. Gate opening has been reported as a particular case of structure flexibility, in which the pore opening occurs at a specific pressure per adsorbate, allowing to use of the difference in onset pressure as a separation mechanism. Examples of this phenomenon are reported in several M'MOFs and STAM-1 [38,39]. Due to the multiple modes of flexibility and MOF response to different external stimuli, the beneficial effect of structural flexibility should be analyzed on a case basis.

Here we compare the adsorption mechanisms of two Cu-based MOFs with one-dimensional diffusivity channels, Cu-MOF-74 and URJC-1. The adsorption of light hydrocarbons, methane, ethane, propane, ethene, and propene in Cu-MOF-74 and URJC-1, based on experimental data and computational results is investigated. Synthesis of the materials, structural characterization, and adsorption isotherms are performed and analyzed by calculating the enthalpy of adsorption, binding geometries, and structural optimizations.

Cu-MOF-74 is a variant of the M-MOF-74 family; this family is formed by a set of well-known structures with open M(II) sites with M = Co, Fe, Mg, Mn, Ni, Zn, and Cu [40–45]. They consist of large hexagonal pores of 10–12 Å diameter where the metal clusters propagate in the *c*-axis. This family has been reported for gas separations such as olefin/paraffin [46–48], carbon dioxide/methane [49,50], and acetylene purification [51–53]. The performance of M-MOF-74 for separation is linked to the strong interaction of its exposed metal centers with certain molecules through π-complexation. While other members of this family have been extensively studied, only a few studies include Cu-MOF-74 [49,54,55].

URJC-1 is a recently reported MOF proposed for different catalytic applications [56,57]. This MOF is characterized by its diamond-shaped pores of about 5 Å and accessible Lewis sites. URJC-1 has open Cu(II) sites pentacoordinated with the nitrogen atoms of the tetrazole and imidazole rings.

Ultimately, an unexpected behaviour of URJC-1 is reported. This highly stable MOF presents an induced framework deformation during the adsorption process. This phenomenon is evidenced by the structure optimization under different conditions and supported by the obtained adsorption isotherms of the hydrocarbons and comparison with the experimental results. An accurate description of the URJC-1 phases is reported for the first time and the obtained structures are well characterized. The representation of the synthesized structures can be found in Fig. 1 and Fig. S1 in the Supporting Information (SI).

2. Methodology

2.1. Synthesis of Cu-MOF-74 and URJC-1

All analytical reagents were commercial products and they were used without further purification.

The synthesis procedure of Cu-MOF-74 was slightly modified from the literature [45]. A mixture of 2,5-dihydroxyterephthalic acid (11.2 mmol) and $Cu(NO_3)_2{\cdot}3H_2O$ (24.6 mmol) were added over a 20:1 (v/v) solution of DMF and 2-propanol (250 mL). The reaction vial was capped tightly and placed in an oven at 80 °C during 18 h.

URJC-1 was synthesized following the procedure previously reported [56]. In a typical synthesis, the material was prepared by mixing 1H-imidazole-4,5-tetrazole as the organic ligand and $Cu(NO_3)_2{\cdot}3H_2O$ as the inorganic source in an acidified solution of N,N′-dimethylformamide and acetonitrile as solvents (6 mL, 3:3, v/v). This mixture was heated at 150 °C for 20 h using a heating ratio of 1.5 °C/min.

2.2. Chemical characterization

X-ray powder diffraction (XRD) patterns, Fig. S2 in the SI, were acquired on a PHILIPS X'PERT diffractometer using Cu *Kα* radiation. The data were recorded from 5 to 50° (2Θ) with a resolution of 0.01°. Fourier transform-infrared spectra (FT-IR) on powdered samples were carried out on a Varian 3100 Excalibur Series spectrometer with a resolution of 4 cm^{-1} and 64 scans coupled to an MKII Golden Gate Single Reflection ATR system to acquire spectra in Attenuated Total Reflectance mode.

2.3. Single-gas adsorption measurements

Both adsorbents were analyzed by low-pressure physisorption. Adsorption and desorption hydrocarbons isotherms were collected in a Tristar II 3020 (Micromeritics). Experiments were conducted at 25 °C (298 K) for methane, ethane and ethene and at 30 °C (303 K) for propane and propene. Nitrogen adsorption-desorption isotherms at 77 K were measured using AutoSorb equipment (Quantachrome Instruments). Both MOF samples were degassed under vacuum at 150 °C for 16 h. Nitrogen adsorption isotherms can be found in Fig. S3 in the SI.

2.4. Computational details

Equilibrium adsorption isotherms were calculated using Monte Carlo simulations in the grand canonical ensemble (GCMC) with the aim of comparing them with the experimental results. Simulations were performed using RASPA software [58,59]. Each point of the adsorption isotherms is obtained after 10^5 MC cycles, and the production runs were performed after 10^4 MC equilibration cycles. The frameworks are considered rigid structures during the adsorption, with the atoms placed at the crystallographic positions. URJC-1 was optimized using classical structural minimizations with an empty and pre-loaded structure with different adsorbates. The geometry optimizations were carried out using NPT ensemble allowing independent variation of the cell lengths and the angles. The configurations were selected from the optimization of the original crystal structure, and the minimizations were performed with (one to four) pre-loaded molecules per unit cell corresponding to low loading up to (over)saturation conditions according to the experimental data. The structural minimizations were performed following the

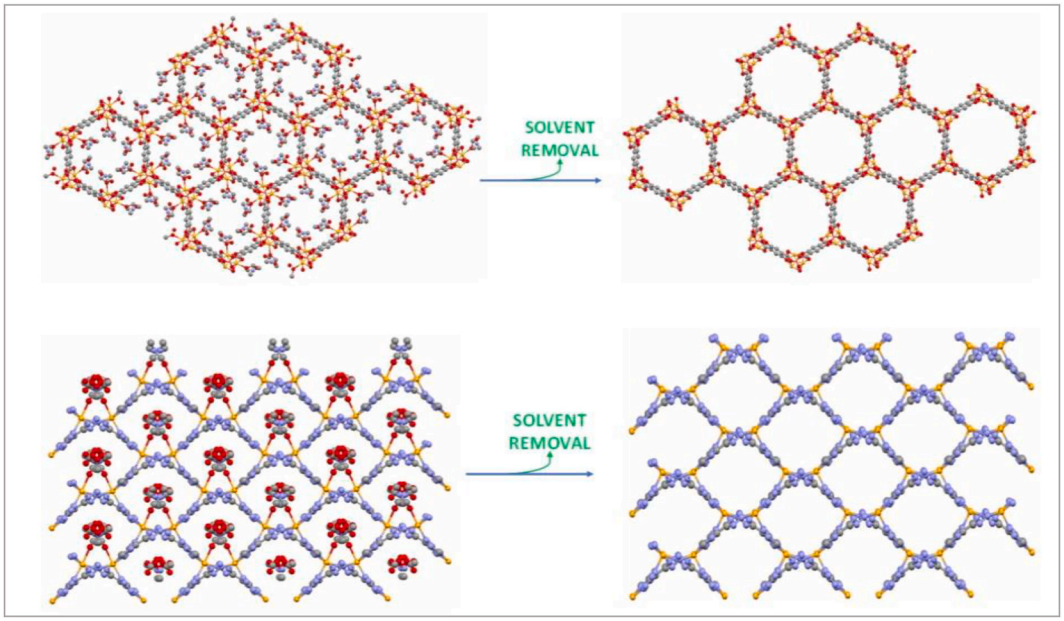

Fig. 1. View along [001] direction of crystal structure of the synthesized materials before and after solvent removal. Cu-MOF-74 (top) and URJC-1 (bottom). Atom color code C = grey, O = red, N = blue, Cu = orange, hydrogen atoms are omitted for clarity.

reported methodology [60,61]. We performed structural characterization of the original crystal structure and the obtained minimizations calculating the pore size distribution (PSD), surface area, and pore volume. Moreover, we carried out energy minimizations using Baker's method [62] in canonical ensemble (NVT) to obtain the binding geometries calculated with a single molecule of the adsorbates in Cu-MOF-74 and URJC-1.

The non-bonded interactions consist of adsorbate-adsorbent and adsorbate-adsorbate van der Waals and electrostatic interactions. The van der Waals interactions are modeled using 12-6 Lennard-Jones potential. The Lennard-Jones parameters for the framework atoms are taken from DREIDING and UFF for the metal atoms [63,64]. The models of the adsorbates are taken from literature. Paraffins are described using a non-charged pseudoatom model where each CH_n group is considered as a single interaction center [65–67]. For olefins, a point charge model is used where partial charges are located in the CH_n_*sp* [2] groups and a point charge is located between the carbon atoms linked by the double bond [68,69]. Lorentz-Berthelot mixing rules are applied to account for the cross interactions. A set of effective point charges is used for the framework atoms. The charges were obtained using EQeq method based on Ewal sums [70]. The resulting charges are listed on Table S1 and the atoms labels shown in Fig. S4 of the SI.

3. Results and discussion

To understand the adsorption mechanisms at the microscopic level, we measured volumetric adsorption isotherms of light hydrocarbons in URJC-1 and Cu-MOF-74.

Figs. 2 and 3 and their semi-logarithmic representations (Figs. S5 and S6) illustrate the behaviour of the two copper adsorbents URJC-1 and Cu-MOF-74 in contact with single-gas hydrocarbon atmospheres under isothermal conditions. URJC-1 presents similar adsorption profiles for both alkane/alkene doublets, Langmuir type isotherms. The adsorption loading intersects at about 1 kPa and show adsorption capacities in a range 2.94–2.96 mol/kg (C2) and 2.38–2.58 mol/kg (C3). The same behaviour is shown for propane and the C2 hydrocarbons in Cu-MOF-74 at higher pressures. However, in URCJ-1 the analysis of adsorption kinetics from the equilibration times reveals the diffusional impediments

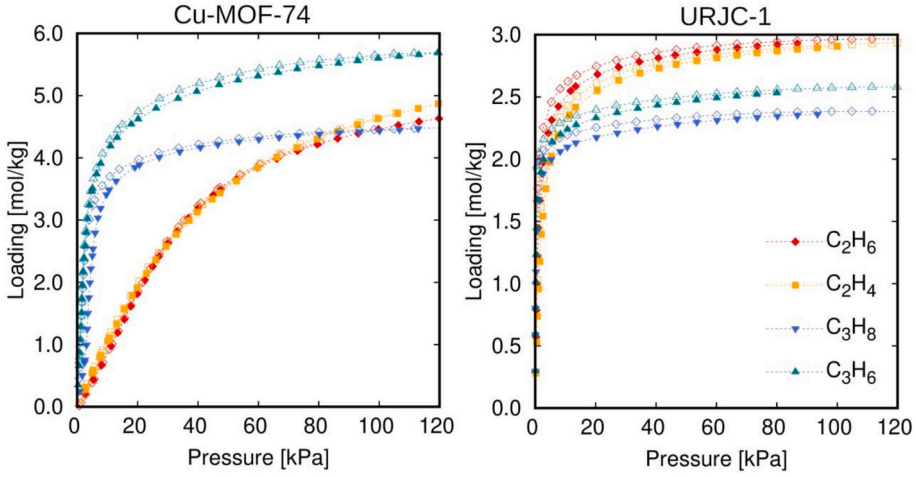

Fig. 2. Low-pressure volumetric adsorption/desorption isotherms of ethane and ethene at 298 K and propane and propene at 303 K. Adsorption (solid symbols) and desorption (open symbols) in Cu-MOF-74 and URJC-1.

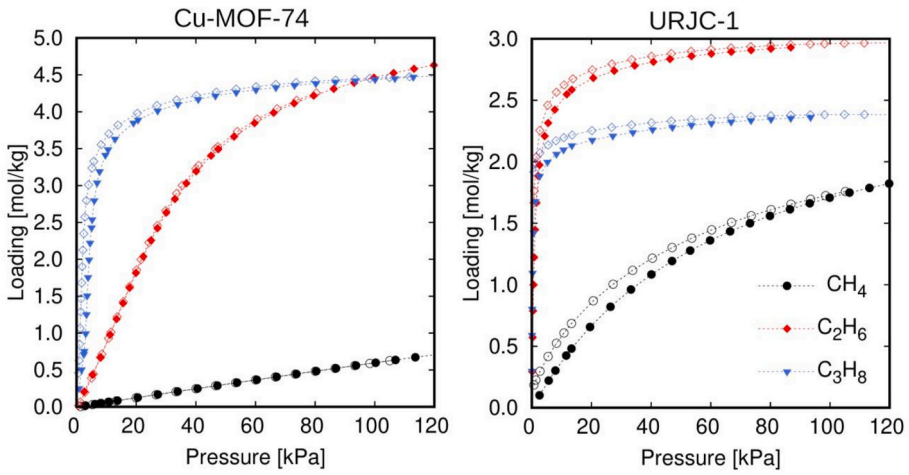

Fig. 3. Low-pressure volumetric adsorption/desorption isotherms of methane, ethane, and propane, at 298 K, 298 K, and 303 K respectively. Adsorption (solid symbols) and desorption (open symbols) in Cu-MOF-74 and URJC-1.

for the alkanes, potentially resulting in a preferential adsorption of olefins in an equimolar mixture. The separation is expected to perform better for the ethane/ethene pair, in which the kinetic limitation is accompanied by a slight displacement on the onset pressure.

Figs. S5 and S6 show the semi-logarithmic representation of the adsorption isotherms and desorption branches. The H2-type hysteresis loop revealed for Cu-MOF-74 evidence some kinetic limitation in the pore necks, thus, the more noticeable hysteresis observed in the largest hydrocarbon (propane) desorption branch is just a confirmation of this effect. On the other hand, URJC-1 exhibits slight hysteresis loops in most of the desorption branches. Its guest-induced structural deformation, and its narrow pores, contribute to this effect. Interaction between adsorbed molecules and the host framework is stronger with longer hydrocarbons producing wider hysteresis loop. The experimental adsorption/desorption raw data and equilibration times are included as Supplementary Information.

Cu-MOF-74 exhibits different profiles for the ethane/ethene and propane/propene couples: despite propane and propene isotherms resemble the URJC-1 results, the adsorption capacities are higher and over a broader pressure range, showing a clearer selectivity towards the alkene. Ethane/ethene curves are almost coincident, with a less steep slope adsorption branch than in URJC-1, hindering the ethane/ethene separation, but allowing a good C2–C3 separation, in that pressure range.

Fig. 3 compares C1, C2, and C3 alkanes adsorption for both MOFs. Methane adsorption capacity is lower than for the other hydrocarbons, particularly in Cu-MOF-74, where the *type III* isotherm is a consequence of low adsorbate-adsorbent interactions. These differences in the adsorption branch, especially in the low-pressure region, evidence a promising potential in adsorptive gas separation processes.

Fig. 4 compares the experimental results for methane, ethane and propane adsorption-desorption uptake and the computed adsorption isotherms obtained using the crystallographic (as-synthesized) structures. The term 'as-synthetized' refers to the experimentally reported structure after removing the solvent. A good agreement between the experimental and simulation adsorption data for Cu-MOF-74 is obtained, with a really accurate result for methane and ethane at 298 K and a slight overestimation for propane adsorption at saturation conditions and 303 K.

As in the case of the paraffins, the computed adsorption isotherms of ethene and propene in Cu-MOF-74 are in good agreement with the experimental data (Fig. 5). Cu-MOF-74 has a remarkably different behaviour compared to that observed for other M-MOF-74 structures. It is well studied and reported that M-MOF-74 is a good candidate for capturing saturated and unsaturated hydrocarbons; the big channels of the MOFs allow high capacity at ambient conditions [71,72]. Because of the π-complexation between the open metal sites (OMS) and the double bond of the olefins, this family of MOFs has also been proposed for alkane/alkene separation [48,73–76]. In this regard, Cu-MOF-74 is an exception; the interaction between the Cu atom and the olefins is weaker than for the other metals, *i.e.,* Co, Fe, Ni, Mg, Mn, and Zn. This behaviour is reflected in the adsorption isotherms of ethene and propene, where the onset pressure in the Cu-based MOF is one order of magnitude higher than for the other metals but shows similar trends in the adsorption of paraffins (Fig. S7). Another difference between Cu-MOF-74 and the remaining M-MOF-74 family members is the capacity. Cu-MOF-74 shows lower loading values at similar conditions, which is consistent with its slightly smaller pore volume. This phenomenon is especially pronounced in the case of olefins (Fig. S7).

On the other hand, the calculated adsorption of methane, ethane, and propane in URJC-1 show a systematic overestimation, especially pronounced for propane. To understand the behaviour of this MOF, structural minimizations were performed on the empty preloaded structures with 1–4 molecules of adsorbate per unit cell, the same final structure is obtained independently of the initial loading, indicating the structural deformation is influenced by the presence of the guest but independent of the adsorbed amount. The calculations are made at intermediate loadings to ensure that the resulting optimized structures are not an artifact of the overestimated saturation capacity. From the energy minimizations two structures are obtained, the empty (URJC-1-e) and loaded (URJC-1-A) structures. The adsorption isotherms of methane, ethane, and propane are computed with both optimized structures. As shown in Fig. 4, the adsorption curves obtained using URJC-1-e are shifted in the pressure range, overestimating the loading over the entire range (open symbols in Fig. 4). Meanwhile, the computed adsorption isotherms of methane and ethane in URJC-1-A are in good agreement with the experimental measurements (solid symbols in Fig. 4).

Given the structural deformation occurred during optimization in presence of the adsorbates and the deviation of the adsorption curves derivated from them, the same approach is used for alkenes. We performed structural optimization of the pre-loaded URJC-1 with alkenes. As a result, a third structure is obtained, URJC-1-B. Adsorption isotherms of ethene and propene were computed for each structure and compared with the experimental measurements (Fig. 5). The adsorption isotherms show an overestimation of the entire curve from 1 to 1.5 mol/kg for ethene and up to 2 mol/kg for propene in URJC-1-e and URJC-1-A. A good agreement, however, was obtained between the experimental observations and calculated adsorption isotherms in URJC-1-B (Fig. 5, full symbols).

In addition to the adsorption isotherms, the adsorption enthalpy as a

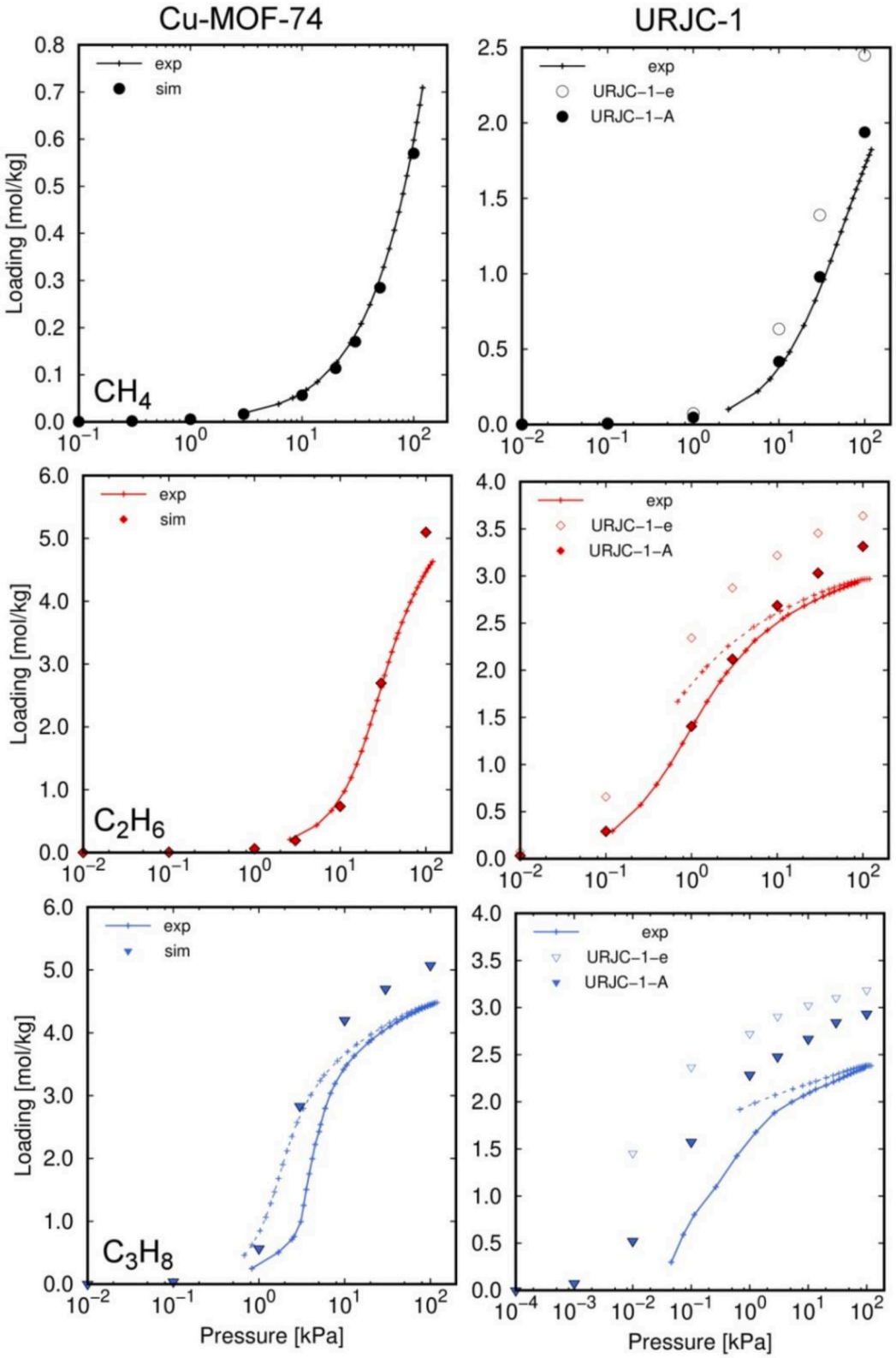

Fig. 4. Single component adsorption isotherms of methane (black circles), ethane (red diamonds) at 298 K, and propane (blue triangles) at 303 K in Cu-MOF-74 and URJC-1. Comparison of experimental adsorption (solid lines) and desorption branches (dashed lines), and calculated adsorption (symbols).

function of the loading using the fluctuation method is calculated [77]. The enthalpy of adsorption follows the expected hierarchy, showing larger interaction with the longer molecules, and the lowest with methane (Fig. 6). The absolute values for the same adsorbate are higher for URJC-1 due to the difference in pore size. The higher interaction between the exposed metal site and the olefins is well reported in the M-MOF-74 analogs and attributed to the π-complexation [78,79]. This phenomenon is also apparent in Cu-based open metal site MOFs [80–83]. However, neither of the MOFs shows evidence of the effect of the open metal sites over the olefins. This is especially noticeable in

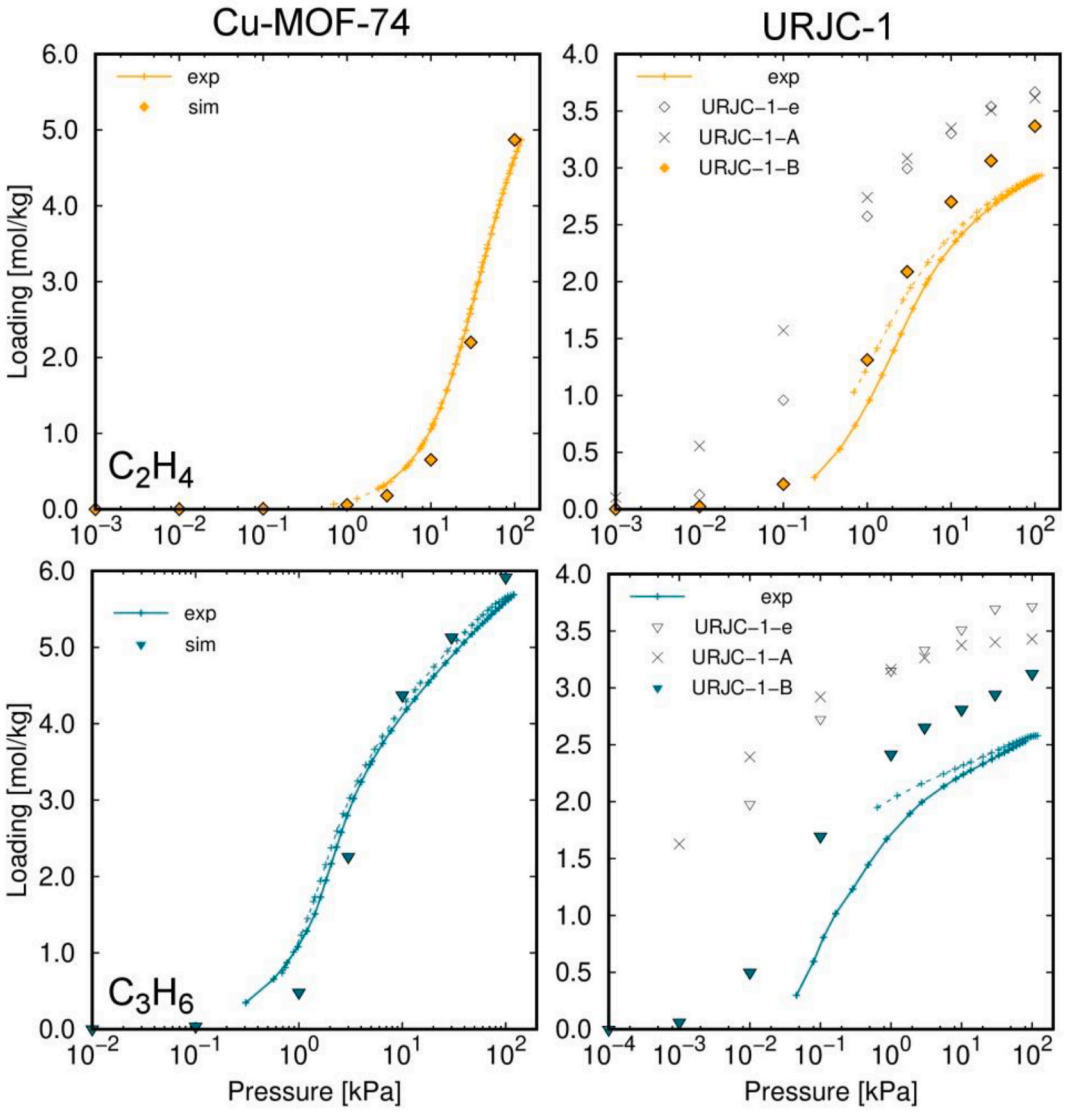

Fig. 5. Single component adsorption isotherms of ethene (*yellow diamonds*) at 298 K and propene (*turquoise triangles*) at 303 K in Cu-MOF-74 and URJC-1. Comparison of experimental adsorption (*solid lines*), desorption branches (*dashed lines*), and calculated adsorption (*symbols*).

Cu-MOF-74 where the dependence of the enthalpy of adsorption as a function of the loading is similar for all the adsorbates, not distinguishing between olefins and paraffins. The exhibited behaviour is in agreement with the trends shown for paraffins in MOF-74 series with different metal centers, reinforcing the conclusion of the lack of π-complexation for the Cu analog.

The binding geometries also show the weaker Cu atoms-double bond interaction observed in the structures under study (Fig. 7). Three parameters are defined to quantify and analyze the binding geometries; the distance between the closest carbon atom to the metal center, l_1; the second closest C–Cu distance, l_2, and the angle between the C–C bond of the adsorbate and the open metal site, α. The parameters are schematically represented in Fig. 7. The hydrocarbon-Cu-MOF-74 binding geometries show considerable longer distances than the other MOFs of the series. This phenomenon was also observed for hydrogen adsorption [84] and carbon dioxide [49], where the Cu-adsorbate interaction is weaker than for the M-MOF-74 analogs. The distance Cu-methane, 3.94 Å, is similar to the reported for Mg-methane, 4 Å [85].

In URJC-1, the molecules are adsorbed in the center of the diffusion channel giving larger Cu–C distances. This phenomenon is caused by the narrow pores that make the center of the cavity the only available adsorption site (Fig. S8). Despite the significant difference in the distances, the orientations of the molecules are similar. It is easy to identify two different behaviour groups; the double bond of ethene and propene faces the Cu atom, and α is between 82 and 85° showing angles typically attributed to the π-complexation. For paraffins, one of the extreme carbon atoms is near the Cu-center forming Cu–C–C angles of 106–110°. These angles are in agreement with those previously reported in the literature [86]. Olefins are placed with the double bond parallel to the metal cluster, while paraffins bind with one extreme carbon atom pointing toward the metal [51].

From this point, the focus is on the structural analysis and characterization of the optimized URJC-1 to understand the consequences of the framework deformation triggered by the adsorbates. The results concerning URJC-1 are calculated with the structure that reproduces the adsorption isotherms, i.e., URJC-1-A for methane, ethane, and propane, and URCJ-1-B for ethene and propene.

The optimized empty structure (URJC-1-e) is practically identical to the crystallographic structure, maintaining pore size, volume, and symmetry, becoming the reference structure. The structures show an almost negligible variation of the lattice parameters, cell lengths, and angles (Table S2), which cannot explain the difference observed in the adsorption. Therefore, the change in the shape of the pores becomes the focus of attention. A set of distances are defined and compared to

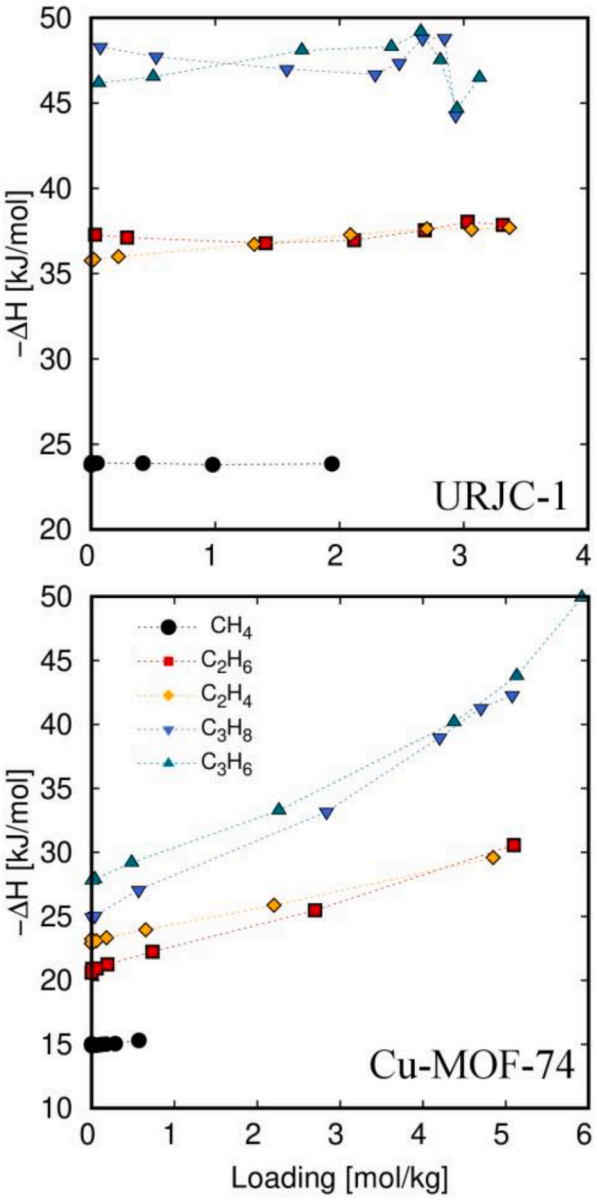

Fig. 6. Enthalpy of adsorption as a function of the loading of methane, ethane, ethene, propane, and propene in URJC-1 and Cu-MOF-74.

account for these differences (Fig. 8). The triangle formed by the in-plane copper atoms defines d_1, d_2, and d_3 distances. URJC-1-A shows a similar increase in the three distances compared to the empty structure. A similar increase is appreciated in d_3 URJC-1-B, while the d_1 increment is twice the obtained for URJC-1-A, and d_2 shows a slight contraction. To understand the implications of the mentioned incremental distances, d_4 and d_5 are also analyzed. d_4 is defined as the distance between the face-to-face Cu atoms, and d_5 is the distance between the faced nitrogen atoms of the tetrazole ring. For URJC-1-A, d_4 is shortened but close to the reference distance, while d_5 is elongated in the same proportions as d_1-d_3. The most significant difference is shown in the elongation of d_4 by URJC-1-B, which is compensated by a contraction in d_5. Finally, the pore deformation can be observed in the torsion angle N–C–C–N, which defines the angle between the planes of the tetrazole and imidazole rings (Fig. S9). The distortion of the diamond-shaped pore is evidenced by minor variations in the configuration of the pores that lead to considerable differences in the adsorption behaviour (Figs. 4 and 5).

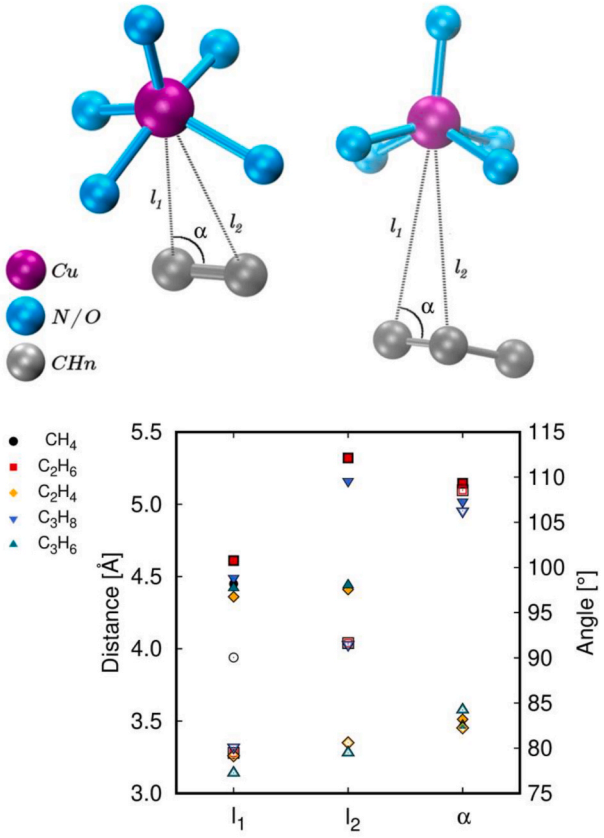

Fig. 7. Schematic representation (*top*) and binding geometry parameters (*bottom*) of CH_n-Cu atoms in URJC-1 (*solid symbols*) and Cu-MOF-74 (*open symbols*).

The deformation of the pores is also reflected in properties such as the pore volume and surface area. Table S3 shows the structural properties of the different URJC-1, surface area, pore volume, and framework density. The calculation of accessible pore volume strongly depends on the probe molecule [87–89]. The pore volume obtained experimentally from the argon adsorption isotherm at 87 K is 0.24 cm^3/g, while the calculated value of the URJC-1-e using helium is 0.32 cm^3/g. To directly compare the values, a correction using the ratio of the van der Waals radii of the probe molecules is needed, 140 and 188 pm for He and Ar atoms, respectively. Table S3 shows the accessible pore volumes using He and Ar atoms as probe molecules and the ones calculated from the experiment. The most significant difference is found between URJC-1 (as synthetized) and URJC-1-e, showing an increase from 0.24 to 0.26 cm^3/g. Nitrogen and argon adsorption isotherms can be found in Fig. S3. The relaxed structure shows larger cell lengths and pore volume, but the preservation of the symmetry and the invariability of the surface area make those changes irrelevant in the adsorption behaviour. This finding reinforces the idea that the diamond-shaped pore distortion is the determinant factor. The adsorption of the hydrocarbons produces a change in the pore shape, causing an increase in the URJC-1 (-A and -B) surface area. The flexibility shown by URJC-1 is very particular when compared with other phase changing MOFs in literature with similar pore size and shape. Although the diamond shape pores of URJC-1 resemble to MIL-53 pores, the two materials behave differently when interacting with adsorbates. MIL-53 exhibits temperature and loading-dependent breathing behaviour, with transitions from narrow to large pores resulting in significant changes in volume (700–1400 $Å^3$), pore size (7.8–13 Å), pore volume (0.07–0.6 cm^3/g), and surface area (non-accessible to 1500 m^2/g) [90–92]. On the other hand, URJC-1 experiences deformation upon interaction with the first adsorbed molecules, but its structure remains unaltered with subsequent adsorbates. The effect in the adsorption in URJC-1 is attributed to the change in

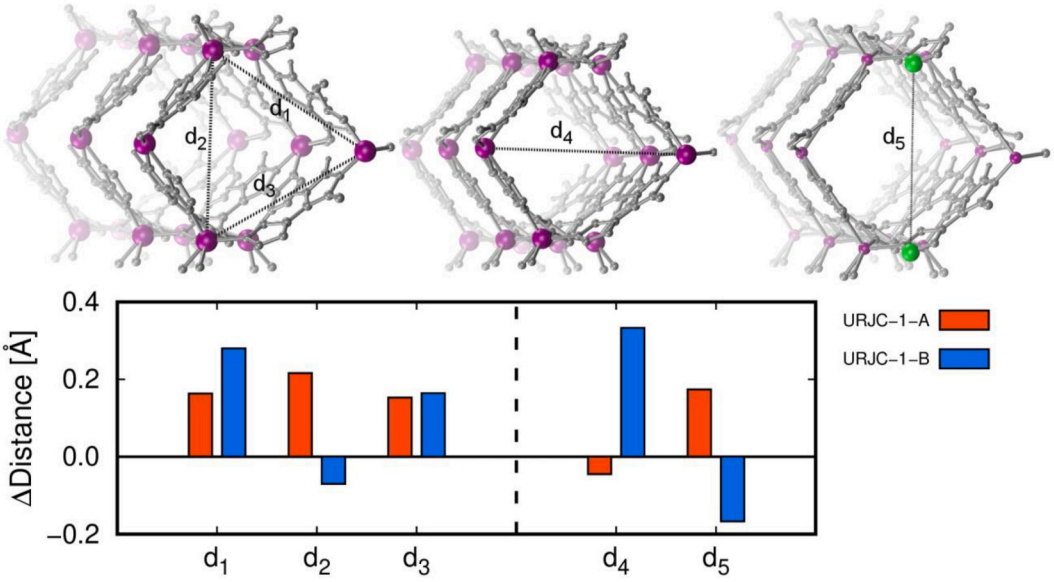

Fig. 8. Schematic representation of atomic connectivity and distance definitions. Copper atoms in violet, nitrogen atoms in green, and the remaining atoms in grey. Incremental distance between the reference structure, URCJ-1-e, and the optimized structures, URJC-1-A and –B.

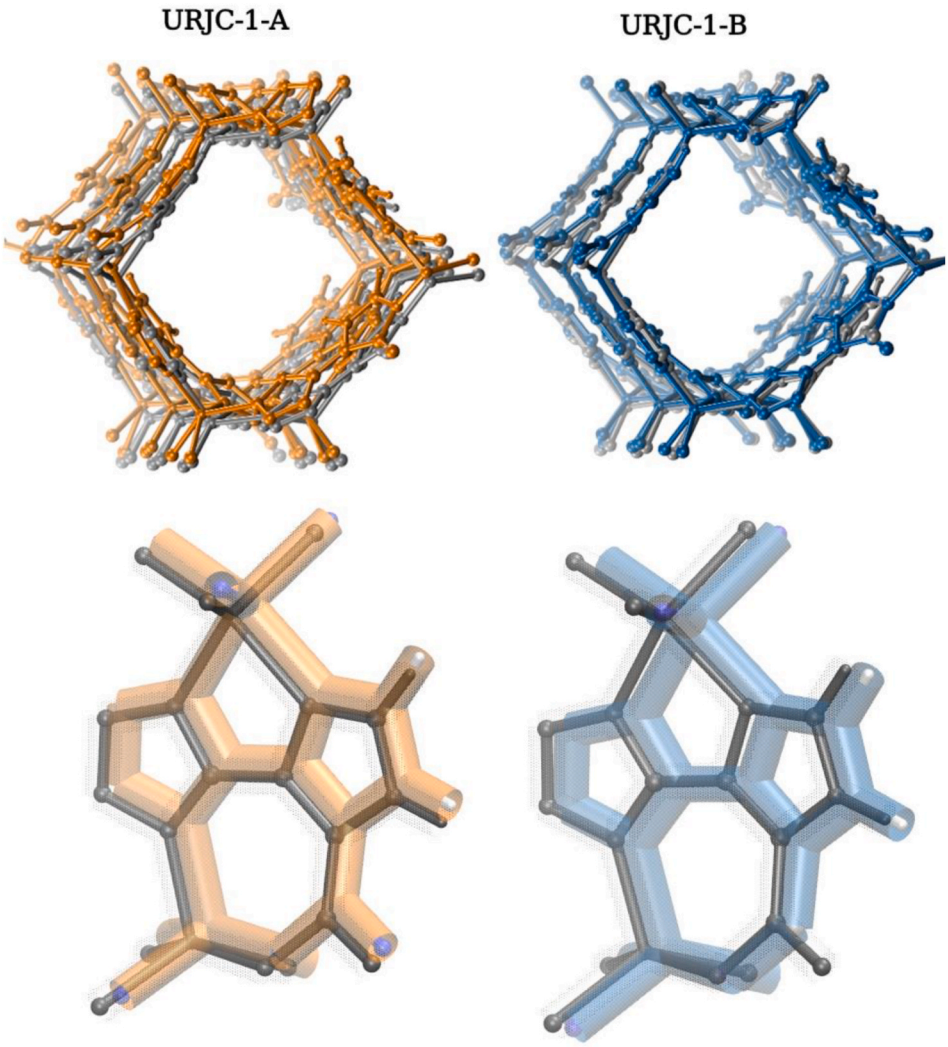

Fig. 9. Schematic representation of the structure deformation of URJC-1-A (orange) and URJC-1-B (blue) compared with the reference structure, URJC-1-e (grey). Single-pore propagation in c-axis (top) and selected fragment (bottom).

diamond shape, rather than significant variations of volume or surface area (Table S3). Further investigation is needed to determine the effect of other external stimuli such as temperature and pressure in the structural deformation of URJC-1. Fig. 9 shows the superposition of the optimized structures URJC-1-A and -B with the reference structure, URJC-1-e. As indicated by the surface areas, the adsorbed paraffins trigger a more pronounced pore distortion. Quantitatively, the variation is shown in the PXRD and pore size distribution (Fig. S10).

4. Conclusions

Two copper-based Metal-Organic Frameworks (Cu-MOF-74 and URJC-1) have been successfully synthesized and characterized. In order to understand their behaviour upon light hydrocarbons adsorption experimental and computational analyses have been performed. Further investigation is needed to determine the potential in gas adsorptive separation processes of these structures.

The results obtained by single-gas adsorption isotherms evidence weaker hydrocarbon-Cu-MOF-74 interactions than the reported in literature for M-MOF-74 analogs. The computational results corroborate the lower impact of Cu in comparison with other metals such as Co, Ni, or Mg, where the difference for alkenes is much more noticeable. In addition, the slightly smaller pore size derives in a lower adsorption capacity.

The results concerning URJC-1 indicate that adsorption occurs in the center of the diffusion channel as a consequence of the narrow pores of the material, providing larger Cu–C distances. Computational analysis reveals the induced framework deformation. A change of the diamond-shaped pores is triggered by the guest molecules affecting the adsorption capacity per adsorbate and the structural properties of the optimized structures. The behaviour of URJC-1 is analyzed and reported in this study for the first time.

The adsorption enthalpies reveals a usual behaviour, higher interaction with larger molecules, following the hierarchy C1<C2<C3. Unexpectedly, the effect of the OMS is negligible in the enthalpy of the olefins; thus, no difference is observed between olefins/paraffins pairs with the same chain length in Cu-MOF-74 and only slight differences at low loading are obtained in URJC-1. Based on the adsorption curves and the energy analysis, we can conclude that tuning operation conditions to the optimal pressure range will allow the use of these copper MOFs in light hydrocarbons mixtures separation processes based on chain length. Whereas the capability of these MOFs to separate olefins from paraffins is not clear and needs further investigation, especially in the case of URJC-1, where the induced deformation of the pores is adsorbate-dependent and could affect the behaviour of the performance in the mixture.

Associated content

The Supporting information includes: XRD patterns of the samples, adsorption isotherms of nitrogen, point charges developed in this work, and structural characterization properties. Other files are included containing the crystallographic information of the optimized structures and the raw adsorption data.

CRediT authorship contribution statement

Azahara Luna-Triguero: Writing – review & editing, Writing – original draft, Visualization, Investigation, Conceptualization. **Eduardo Andres-Garcia:** Writing – review & editing, Writing – original draft, Investigation, Conceptualization. **Pedro Leo:** Writing – review & editing, Writing – original draft, Investigation, Conceptualization. **Willy Rook:** Writing – review & editing. **Freek Kapteijn:** Writing – review & editing, Resources.

Declaration of competing interest

The authors declare the following financial interests/personal relationships which may be considered as potential competing interests: Pedro Leo and Eduardo Andres-Garcia reports financial support was provided by Spain Ministry of Science and Innovation. The authors declare no conflict of interest.

Data availability

Data will be made available on request.

Acknowledgments

The authors thank the Spanish Ministry of Science and Innovation and the Spanish State Research Agency for the financial support (ProjectPGC2018-099296-B-I00). This work is supported by the Irene Curie Fellowship (ICF). E. A.-G thanks MICINN for a Juan de la Cierva Formación fellowship (FJC2019-039015-I) and Margarita Salas fellowship (MS21-035).

Appendix A. Supplementary data

Supplementary data to this article can be found online at https://doi.org/10.1016/j.micromeso.2023.112699.

References

[1] R. Hafezi, A. Akhavan, S. Pakseresht, D.A. Wood, Global natural gas demand to 2025: a learning scenario development model, Energy 224 (2021), 120167.
[2] R.M. Flores, Coalbed methane: from hazard to resource, Int. J. Coal Geol. 35 (1998) 3–26.
[3] R. van Wissen, M. Golombok, J. Brouwers, Separation of carbon dioxide and methane in continuous countercurrent gas centrifuges, Chem. Eng. Sci. 60 (2005) 4397–4407.
[4] R.W. Howarth, R. Santoro, A. Ingraffea, Methane and the greenhouse-gas footprint of natural gas from shale formations, Climatic Change 106 (2011) 679–690.
[5] J.S. Plotkin, A. Nizamoff, The changing dynamics of olefin supply/demand, Catal. Today 106 (2008).
[6] D.M. Ruthven, S. Farooq, K.S. Knaebel, Pressure Swing Adsorption, VCH, 1994.
[7] P. Krokidas, M. Castier, S. Moncho, E. Brothers, I.G. Economou, Molecular simulation studies of the diffusion of methane, ethane, propane, and propylene in ZIF-8, J. Phys. Chem. C 119 (2015) 27028–27037.
[8] L. Rollins, Economic Impacts and Market Challenges for the Methane to Derivatives Petrochemical Sub-sector, 2018.
[9] T. Ren, M. Patel, K. Blok, Olefins from conventional and heavy feedstocks: energy use in steam cracking and alternative processes, Energy 31 (2006) 425–451.
[10] D.J. Safarik, R.B. Eldridge, Olefin/paraffin separations by reactive absorption: a review, Ind. Eng. Chem. Res. 37 (1998) 2571–2581.
[11] J.-R. Li, J. Sculley, H.-C. Zhou, Metal–organic frameworks for separations, Chem. Rev. 112 (2012) 869–932, https://doi.org/10.1021/cr200190s.
[12] H. Montes-Andrés, et al., Novel and versatile cobalt Azobenzene-based metal-organic framework as hydrogen adsorbent, ChemPhysChem 20 (2019) 1334–1339.
[13] L. Wang, et al., Metal–organic frameworks for energy storage: batteries and supercapacitors, Coord. Chem. Rev. 307 (2016) 361–381.
[14] P. Horcajada, et al., Metal–organic frameworks in biomedicine, Chem. Rev. 112 (2012) 1232–1268, https://doi.org/10.1021/cr200256v.
[15] K. Ni, et al., Nanoscale metal-organic frameworks for x-ray activated in situ cancer vaccination, Sci. Adv. 6 (2020), eabb5223.
[16] Y. Cui, Y. Yue, G. Qian, B. Chen, Luminescent functional metal–organic frameworks, Chem. Rev. 112 (2012) 1126–1162.
[17] N. Stock, S. Biswas, Synthesis of metal-organic frameworks (MOFs): routes to various MOF topologies, morphologies, and composites, Chem. Rev. 112 (2012) 933–969.
[18] Y. Bai, et al., Zr-based metal–organic frameworks: design, synthesis, structure, and applications, Chem. Soc. Rev. 45 (2016) 2327–2367.
[19] R. Salunkhe, Y. Kaneti, J. Kim, J. Yamauchi Kim, Y1: CAS: 528: DC% 2BC28XhvFelu7bJ: nanoarchitectures for metal-organic framework-derived nanoporous carbons toward supercapacitor applications, Acc. Chem. Res. 49 (2016) 2796–2806.
[20] B. Li, et al., Emerging multifunctional metal–organic framework materials, Adv. Mater. 28 (2016) 8819–8860.
[21] H. Kim, C.S. Hong, MOF-74-type frameworks: tunable pore environment and functionality through metal and ligand modification, CrystEngComm 23 (2021) 1377–1387, https://doi.org/10.1039/d0ce01870h.
[22] Cambridge database. https://www.ccdc.cam.ac.uk.

[23] P.Z. Moghadam, et al., Targeted classification of metal–organic frameworks in the Cambridge structural database (CSD), Chem. Sci. 11 (2020) 8373–8387.
[24] M.L. Foo, et al., An adsorbate discriminatory gate effect in a flexible porous coordination polymer for selective adsorption of CO2 over C2H2, J. Am. Chem. Soc. 138 (2016) 3022–3030.
[25] L. Li, et al., Flexible–robust metal–organic framework for efficient removal of propyne from propylene, J. Am. Chem. Soc. 139 (2017) 7733–7736, https://doi.org/10.1021/jacs.7b04268.
[26] S. Couck, et al., Adsorption and separation of light gases on an Amino-functionalized metal–organic framework: an adsorption and in situ XRD study, ChemSusChem 5 (2012) 740–750.
[27] P. Serra-Crespo, R. Berger, W. Yang, J. Gascon, F. Kapteijn, Separation of CO2/CH4 mixtures over NH2-MIL-53—an experimental and modelling study, Chem. Eng. Sci. 124 (2015) 96–108.
[28] P. Serra-Crespo, et al., Preliminary design of a vacuum pressure swing adsorption process for natural gas upgrading based on Amino-functionalized MIL-53, Chem. Eng. Technol. 38 (2015) 1183–1194.
[29] S. Horike, S. Shimomura, S. Kitagawa, Soft porous crystals, Nat. Chem. 1 (2009) 695–704, https://doi.org/10.1038/nchem.444.
[30] G. Ferey, C. Serre, Large breathing effects in three-dimensional porous hybrid matter: facts, analyses, rules and consequences, Chem. Soc. Rev. 38 (2009) 1380–1399, https://doi.org/10.1039/b804302g.
[31] S. Kitagawa, R. Kitaura, S. Noro, Functional porous coordination polymers, Angew. Chem. Int. Ed. 43 (2004) 2334–2375, https://doi.org/10.1002/anie.200300610.
[32] A. Schneemann, et al., Flexible metal-organic frameworks, Chem. Soc. Rev. 43 (2014) 6062–6096, https://doi.org/10.1039/c4cs00101j.
[33] Y. Yang, D.S. Sholl, A systematic examination of the impacts of MOF flexibility on intracrystalline molecular diffusivities, J. Mater. Chem. 10 (2022) 4242–4253, https://doi.org/10.1039/d1ta09267g.
[34] M. Maes, et al., Separation of styrene and ethylbenzene on metal− organic frameworks: analogous structures with different adsorption mechanisms, J. Am. Chem. Soc. 132 (2010) 15277–15285.
[35] H.-M. Wen, B. Li, H. Wang, R. Krishna, B. Chen, High acetylene/ethylene separation in a microporous zinc(ii) metal–organic framework with low binding energy, Chem. Commun. 52 (2016) 1166–1169, https://doi.org/10.1039/c5cc08210b.
[36] K. Kishida, et al., Structural optimization of interpenetrated pillared-layer coordination polymers for ethylene/ethane separation, Chem.–Asian J. 9 (2014) 1643–1647.
[37] R. Chen, et al., Sequential separation of linear, mono-, and Di-branched hexane isomers on a robust coordination polymer with nonbonding flexibility, Small (2023), 2207367.
[38] M.C. Das, et al., Interplay of metalloligand and organic ligand to tune micropores within isostructural mixed-metal organic frameworks (M′ MOFs) for their highly selective separation of chiral and achiral small molecules, J. Am. Chem. Soc. 134 (2012) 8703–8710.
[39] A. Sławek, et al., Gate-opening mechanism of hydrophilic–hydrophobic metal–organic frameworks: molecular simulations and Quasi-equilibrated desorption, Chem. Mater. 30 (2018) 5116–5127.
[40] N.L. Rosi, et al., Rod packings and metal-organic frameworks constructed from rod-shaped secondary building units, J. Am. Chem. Soc. 127 (2005) 1504–1518.
[41] P.D. Dietzel, Y. Morita, R. Blom, H. Fjellvåg, An in situ high temperature single crystal investigation of a Dehydrated metal-organic framework compound and field-induced magnetization of one-dimensional metal-oxygen chains, Angew. Chem. 117 (2005) 6512–6516.
[42] P.D.C. Dietzel, B. Panella, M. Hirscher, R. Blom, H. Fjellvag, Hydrogen adsorption in a nickel based coordination polymer with open metal sites in the cylindrical cavities of the desolvated framework, Chem. Commun. (2006) 959–961, https://doi.org/10.1039/b515434k.
[43] W. Zhou, H. Wu, T. Yildirim, Enhanced H-2 adsorption in isostructural metal-organic frameworks with open metal sites: strong dependence of the binding strength on metal ions, J. Am. Chem. Soc. 130 (2008) 15268–15269, https://doi.org/10.1021/ja807023q.
[44] S. Bhattacharjee, et al., Solvothermal synthesis of Fe-MOF-74 and its catalytic properties in phenol hydroxylation, J. Nanosci. Nanotechnol. 10 (2010) 135–141, https://doi.org/10.1166/jnn.2010.1493.
[45] R. Sanz, F. Martínez, G. Orcajo, L. Wojtas, D. Briones, Synthesis of a honeycomb-like Cu-based metal–organic framework and its carbon dioxide adsorption behaviour, Dalton Trans. 42 (2013) 2392–2398.
[46] P. Mishra, S. Edubilli, B. Mandal, S. Gumma, Adsorption characteristics of metal organic frameworks containing coordinatively unsaturated metal sites: effect of metal cations and adsorbate properties, J. Phys. Chem. C 118 (2014) 6847–6855, https://doi.org/10.1021/jp412622b.
[47] E.D. Bloch, et al., Hydrocarbon separations in a metal-organic framework with open iron(II) coordination sites, Science 335 (2012) 1606–1610, https://doi.org/10.1126/science.1217544.
[48] S.J. Geier, et al., Selective adsorption of ethylene over ethane and propylene over propane in the metal-organic frameworks M-2(dobdc) (M = Mg, Mn, Fe, Co, Ni, Zn), Chem. Sci. 4 (2013) 2054–2061, https://doi.org/10.1039/c3sc00032j.
[49] W.L. Queen, et al., Comprehensive study of carbon dioxide adsorption in the metal–organic frameworks M 2 (dobdc)(M= Mg, Mn, Fe, Co, Ni, Cu, Zn), Chem. Sci. 5 (2014) 4569–4581.
[50] E. Haldoupis, et al., Ab initio derived force fields for predicting CO2 adsorption and Accessibility of metal sites in the metal–organic frameworks M-MOF-74 (M = Mn, Co, Ni, Cu), J. Phys. Chem. C 119 (2015) 16058–16071, https://doi.org/10.1021/acs.jpcc.5b03700.
[51] Y. He, R. Krishna, B. Chen, Metal-organic frameworks with potential for energy-efficient adsorptive separation of light hydrocarbons, Energy Environ. Sci. 5 (2012) 9107–9120, https://doi.org/10.1039/c2ee22858k.
[52] X.-J. Hou, P. He, H. Li, X. Wang, Understanding the adsorption mechanism of C2H2, CO2, and CH4 in isostructural metal–organic frameworks with coordinatively unsaturated metal sites, J. Phys. Chem. C 117 (2013) 2824–2834, https://doi.org/10.1021/jp310517r.
[53] A. Luna-Triguero, J.M. Vicent-Luna, R.M. Madero-Castro, P. Gómez-Álvarez, S. Calero, Acetylene storage and separation using metal–organic frameworks with open metal sites, ACS Appl. Mater. Interfaces 11 (2019) 31499–31507, https://doi.org/10.1021/acsami.9b09010.
[54] T. Stolar, et al., Scalable mechanochemical amorphization of bimetallic Cu− Zn MOF-74 catalyst for selective CO2 reduction reaction to methanol, ACS Appl. Mater. Interfaces 13 (2021) 3070–3077.
[55] M.J. Katz, et al., High volumetric uptake of ammonia using Cu-MOF-74/Cu-CPO-27, Dalton Trans. 45 (2016) 4150–4153, https://doi.org/10.1039/c5dt03436a.
[56] P. Leo, et al., New URJC-1 material with remarkable stability and acid-base catalytic properties, Polymers 8 (2016) 44.
[57] A. Muñoz, P. Leo, G. Orcajo, F. Martínez, G. Calleja, URJC-1-MOF as new heterogeneous recyclable catalyst for C-heteroatom coupling reactions, ChemCatChem 11 (2019) 3376–3380.
[58] D. Dubbeldam, A. Torres-Knoop, K.S. Walton, On the inner workings of Monte Carlo codes, Mol. Simulat. 39 (2013) 1253–1292, https://doi.org/10.1080/08927022.2013.819102.
[59] D. Dubbeldam, S. Calero, D.E. Ellis, R.Q. Snurr, RASPA: molecular simulation software for adsorption and diffusion in flexible nanoporous materials, Mol. Simulat. 42 (2015) 81–101, https://doi.org/10.1080/08927022.2015.1010082.
[60] D. Dubbeldam, R. Krishna, R. Snurr, Method for analyzing structural changes of flexible metal− organic frameworks induced by adsorbates, J. Phys. Chem. C 113 (2009) 19317–19327.
[61] A. Luna-Triguero, J.M. Vicent-Luna, S. Calero, Phase transition induced by gas adsorption in metal-organic frameworks, Chem.–Eur. J. 24 (2018) 8530–8534.
[62] J. Baker, An algorithm for the location of transition states, J. Comput. Chem. 7 (1986) 385–395.
[63] S.L. Mayo, B.D. Olafson, W.A. Goddard, Dreiding - a generic force-field for molecular simulations, J. Phys. Chem. 94 (1990) 8897–8909, https://doi.org/10.1021/j100389a010.
[64] A.K. Rappe, C.J. Casewit, K.S. Colwell, W.A. Goddard, W.M. Skiff, UFF, a full periodic-table force-field for molecular mechanics and molecular-dynamics simulations, J. Am. Chem. Soc. 114 (1992) 10024–10035, https://doi.org/10.1021/ja00051a040.
[65] A. García-Sánchez, E. García-Pérez, D. Dubbeldam, R. Krishna, S. Calero, A simulation study of alkanes in Linde Type A zeolites, Adsorpt. Sci. Technol. 25 (2007) 417–427.
[66] D. Dubbeldam, et al., United atom force field for alkanes in nanoporous materials, J. Phys. Chem. B 108 (2004) 12301–12313, https://doi.org/10.1021/jp0376727.
[67] J.J. Potoff, J.I. Siepmann, Vapor–liquid equilibria of mixtures containing alkanes, carbon dioxide, and nitrogen, AIChE J. 47 (2001) 1676–1682.
[68] J.J. Gutiérrez-Sevillano, et al., Analysis of the ITQ-12 zeolite performance in propane− propylene separations using a combination of experiments and molecular simulations, J. Phys. Chem. C 114 (2010) 14907–14914.
[69] T.M. Becker, et al., Potential of polarizable force fields for predicting the separation performance of small hydrocarbons in M-MOF-74, Phys. Chem. Chem. Phys. 20 (2018) 28848–28859.
[70] C.E. Wilmer, K.C. Kim, R.Q. Snurr, An extended charge equilibration method, J. Phys. Chem. Lett. 3 (2012) 2506–2511.
[71] A. Liu, et al., Adsorption and diffusion of benzene in Mg-MOF-74 with open metal sites, ACS Appl. Mater. Interfaces 11 (2019) 4686–4700.
[72] Z. Bao, et al., Adsorption of ethane, ethylene, propane, and propylene on a magnesium-based metal–organic framework, Langmuir 27 (2011) 13554–13562, https://doi.org/10.1021/la2030473.
[73] P. Verma, X.F. Xu, D.G. Truhlar, Adsorption on Fe-MOF-74 for C1-C3 hydrocarbon separation, J. Phys. Chem. C 117 (2013) 12648–12660, https://doi.org/10.1021/jp402884h.
[74] A. Luna-Triguero, et al., Effective model for olefin/paraffin separation using (Co, Fe, Mn, Ni)-MOF-74, ChemistrySelect 2 (2017) 665–672, https://doi.org/10.1002/slct.201601095.
[75] H. Sun, et al., Tuning 1-hexene/n-hexane adsorption on MOF-74 via constructing Co-Mg bimetallic frameworks, Microporous Mesoporous Mater. 284 (2019) 151–160.
[76] B.L. Suh, T. Hyun, D.-Y. Koh, J. Kim, Rational tuning of ultramicropore Dimensions in MOF-74 for size-selective separation of light hydrocarbons, Chem. Mater. 33 (2021) 7686–7692.
[77] A. Torres-Knoop, A. Poursaeidesfahani, T.J. Vlugt, D. Dubbeldam, Behavior of the enthalpy of adsorption in nanoporous materials close to saturation conditions, J. Chem. Theor. Comput. 13 (2017) 3326–3339.
[78] H. Kim, J. Park, Y. Jung, The binding nature of light hydrocarbons on Fe/MOF-74 for gas separation, Phys. Chem. Chem. Phys. 15 (2013) 19644–19650, https://doi.org/10.1039/c3cp52980k.
[79] H. Abedini, A. Shariati, M.R. Khosravi-Nikou, Adsorption of propane and propylene on M-MOF-74 (M= Cu, Co): equilibrium and kinetic study, Chem. Eng. Res. Des. 153 (2020) 96–106.
[80] M.H. Mohamed, et al., Designing open metal sites in metal–organic frameworks for paraffin/olefin separations, J. Am. Chem. Soc. 141 (2019) 13003–13007.

[81] A.R. Kulkarni, D.S. Sholl, Screening of copper open metal site MOFs for olefin/paraffin separations using DFT-derived force fields, J. Phys. Chem. C 120 (2016) 23044–23054, https://doi.org/10.1021/acs.jpcc.6b07493.
[82] A.F.P. Ferreira, et al., Suitability of Cu-BTC extrudates for propane-propylene separation by adsorption processes, Chem. Eng. J. 167 (2011) 1–12, https://doi.org/10.1016/j.cej.2010.07.041.
[83] A. Luna-Triguero, J.M. Vicent-Luna, P. Gómez-Álvarez, S. Calero, Olefin/paraffin separation in open metal site Cu-BTC metal–organic framework, J. Phys. Chem. C 121 (2017) 3126–3132, https://doi.org/10.1021/acs.jpcc.6b11808.
[84] M.H. Rosnes, et al., Intriguing differences in hydrogen adsorption in CPO-27 materials induced by metal substitution, J. Mater. Chem. 3 (2015) 4827–4839, https://doi.org/10.1039/c4ta05794e.
[85] K. Sillar, J. Sauer, Ab initio prediction of adsorption isotherms for small molecules in metal–organic frameworks: the effect of lateral interactions for methane/CPO-27-Mg, J. Am. Chem. Soc. 134 (2012) 18354–18365, https://doi.org/10.1021/ja307076t.
[86] K. Lee, J.D. Howe, L.-C. Lin, B. Smit, J.B. Neaton, Small-molecule adsorption in open-site metal–organic frameworks: a systematic density functional theory study for rational design, Chem. Mater. 27 (2015) 668–678.
[87] M.F. De Lange, T.J. Vlugt, J. Gascon, F. Kapteijn, Adsorptive characterization of porous solids: error analysis guides the way, Microporous Mesoporous Mater. 200 (2014) 199–215.
[88] M.F. De Lange, L.-C. Lin, J. Gascon, T.J. Vlugt, F. Kapteijn, Assessing the surface area of porous solids: limitations, probe molecules, and methods, Langmuir 32 (2016) 12664–12675.
[89] J. Osterrieth, et al., How Reproducible Are Surface Areas Calculated from the BET Equation?, 2022.
[90] A. Boutin, et al., The behavior of flexible MIL-53(Al) upon CH4 and CO2 adsorption, J. Phys. Chem. C 114 (2010) 22237–22244, https://doi.org/10.1021/jp108710h.
[91] F.-X. Coudert, et al., Water adsorption in flexible gallium-based MIL-53 metal–organic framework, J. Phys. Chem. C 118 (2014) 5397–5405, https://doi.org/10.1021/jp412433a.
[92] P. Horcajada, et al., Flexible porous metal-organic frameworks for a controlled drug Delivery, J. Am. Chem. Soc. 130 (2008) 6774–6780, https://doi.org/10.1021/ja710973k.